Computers & Fluids 40 (2011) 179–187

Contents lists available at ScienceDirect

Computers & Fluids

journal homepage: www.elsevier.com/locate/compfluid

Temporal/spatial simulation of the stratified far wake of a sphere

R. Pasquetti

Lab. J.A. Dieudonné, UMR CNRS 6621, University of Nice-Sophia Antipolis, Parc Valrose, 06108 Nice Cedex 2, France

ARTICLE INFO

Article history:
Received 29 March 2010
Received in revised form 8 July 2010
Accepted 31 August 2010
Available online 21 September 2010

Keywords:
Wake flows
Stratified fluids
Large-eddy simulation
Spectral vanishing viscosity
Spectral methods

ABSTRACT

Far wakes are generally studied on the basis of a temporal development study, *i.e.* the flow is assumed periodic in streamwise direction and one focuses on its evolution in time. It is then required to set up an appropriate initial condition to start the calculation. Like in some previous works, we study the far wake of a sphere in a stratified fluid, but rather than starting from an *ad hoc* initial condition, we first carry out a spatial development simulation in order to define a relevant initialization. The control parameters of the flow are the Prandtl, Reynolds and internal Froude numbers, that we take equal to $Pr = 7$, $Re = 10{,}000$ and $F = 25$. The numerical method is based on a spectral multi-domain Fourier–Chebyshev approximation, stabilized by using a spectral vanishing viscosity technique, that may be interpreted as a spectral large-eddy simulation closure restricted to the high frequencies. Very realistic results are obtained, especially showing the so-called three-dimensional (3D), non-equilibrium (NEQ) and quasi two-dimensional (Q2D) regimes, with satisfactory comparisons with the experiments.

1. Introduction

Wakes in stratified fluids have now a long history, as *e.g.* summarized in [1,2] and references herein. Simulating such flows, especially when they are turbulent, remains however a challenging task. The smallest scales of the flow are generally out of reach of Direct Numerical Simulation (DNS), and so it is required to use Reynolds Averaged Navier–Stokes (RANS) or Large-Eddy Simulations (LES) approaches, the latter being better adapted to a detailed description of the flow. Moreover, the computation of far wakes cannot be achieved in very elongated domain, so that the simulations are generally based on temporal development studies.

Stratified fluids are essentially characterized by the Brunt Väisälä angular frequency N, such that $N^2 = -g\partial_y\rho/\rho$, where y denotes the vertical axis, ρ the fluid density and g the gravity acceleration. In case of a thermal stratification, if the variations of $\rho(y)$ are weak, then with α for the thermal expansion coefficient $N^2 \approx g\alpha\partial_y T_0$, where T_0 is the basis temperature profile. Hereafter we suppose that the stratification is linear ($\partial_y T_0 = cte > 0$). In the frame of wake flows, from the buoyancy frequency arises the dimensionless internal Froude number: With D, U and $\delta T = D\partial_y T_0$, for a characteristic length, velocity and temperature gap, respectively, one has $F = U/(ND)$. For given Reynolds and Péclet numbers, depending on the value of F a large variety of flows may be obtained, see *e.g.* [3,4] for the wake of a sphere of velocity U and diameter D. Note that for both the sphere and the cylinder, some authors prefer to define the Froude number with the radius, say R, so that with obvious notations, $F_R = 2F$.

Here we consider the turbulent wake of a towed sphere in thermally stratified water. Experimental results in this case are numerous, see *e.g.* [5–7]. The Reynolds, internal Froude and Prandtl numbers are taken equal to $Re = UD/\nu = 10^4$, where ν is the kinematic viscosity, $F = U/(ND) = 25$ and $Pr = \nu/\kappa = 7$, where κ is the thermal diffusivity, respectively. Note that $N = 5 \times 10^{-3}$ rd s^{-1} is typical of a thermal stratification in the oceans. We are especially interested in the very late wake, *i.e.* at distances $l \sim 2500D$ from the sphere, or equivalently, using $1/N$ as reference time, after a dimensionless time delay $Nt = l/(FD) \sim 100$. Computations similar to the one proposed here were *e.g.* carried out in [8–10], but these studies only provide a temporal study: The flow is assumed periodic in longitudinal direction and the initial conditions, for velocity and temperature, correspond to mean profiles with superimposition of an *ad hoc* noise, issued from first and second order statistics of some experiments. In this case, no coherent structures are present in the flow at the initial time and so the validity of the temporal study may be criticized. Especially, phase coherence is not maintained and one observes significant transients in start-up due to the mismatch of forcing and correct Navier–Stokes solutions. In the present work we first carry out a computation of the spatial development, so that we can start the temporal study with a relevant initial condition.

The paper is structured as follows. In Section 2 we briefly describe the model and the numerical method and also give some details on our Spectral Vanishing Viscosity–Large-Eddy Simulation (SVV–LES) approach. In Section 3 we describe the space development study and provide some statistics on the computed

E-mail address: Richard.PASQUETTI@unice.fr

0045-7930/$ - see front matter © 2010 Elsevier Ltd. All rights reserved.
doi:10.1016/j.compfluid.2010.08.023

flow. In Section 4 we explain how we extend the spatial development computation by a temporal development study. Detailed results and comparisons with the experiments are given in Section 5.

2. Modeling and numerical method

2.1. Modeling

The flow is assumed to be governed by the incompressible Navier–Stokes equations coupled, within the Boussinesq approximation, to an advection–diffusion equation for the temperature. In dimensionless form these equations are:

$$D_t\boldsymbol{u} = -\nabla p + \frac{1}{F^2}T\boldsymbol{e}_y + \frac{1}{Re}\Delta\boldsymbol{u} \tag{1}$$

$$\nabla\cdot\boldsymbol{u} = 0 \tag{2}$$

$$D_t T = \frac{1}{Pe}\Delta T \tag{3}$$

where t is the time, D_t the material derivative, $\boldsymbol{e}_y$ the unit vector in vertical direction y, $\boldsymbol{u}$, p and T the velocity, pressure and temperature fields, respectively. For the reference length, velocity, time, temperature and pressure we use D, U, D/U, $D\partial_y T_0$ and ρU^2, respectively (D, sphere diameter, U, sphere velocity, $\partial_y T_0$, initial vertical gradient and ρ, density). The control parameters of the flow are the Reynolds ($Re = UD/\nu$), Péclet ($Pe = UD/\kappa$) and internal Froude ($F = U/(ND)$) numbers.

We are interested in the far wake of a sphere moving at constant velocity in an open domain stably stratified with a constant vertical temperature gradient. From practical considerations, the computational domain must however be bounded and artificial boundary conditions have then to be introduced, as described in Sections 3 and 5 for the spatial and temporal studies, respectively. At the surface of the sphere the no slip condition is relevant and for the temperature this is discussed in next Section.

2.2. Numerical method

The governing equations are considered in a parallelepiped domain, aligned on the axis of the Cartesian coordinate system, with x for the longitudinal streamwise direction, y for the vertical direction and z for the horizontal transverse direction, which is assumed homogeneous. A domain decomposition technique with conforming meshes is implemented in the elongated x-streamwise direction. In each subdomain one uses a Chebyshev–Fourier spectral approximation, *i.e.* Chebyshev expansions are used in the x-streamwise and y-vertical directions, while Fourier expansions are used in the z-transverse direction. In z-direction the width of the domain is chosen sufficiently large to avoid any coupling.

The time scheme is second order accurate and makes use of three (resp. two) steps for the velocity (resp. temperature): A transport step, a diffusion step and, for the velocity, a projection step yielding a divergence-free vector field. The transport step is handled explicitly, using an Operator Integration Factor (OIF) semi-Lagrangian method and the RK4 scheme. The diffusion step is handled implicitly, using BDF2, *i.e.* the material derivative is approximated by using a three-level backward finite difference scheme. The projection step allows to obtain the velocity field by solving a 'pseudo-Poisson' problem for the pressure correction, using the so-called $P_N - P_{N-2}$ approximation, so that the pressure correction problem is well posed and no boundary conditions are required for the pressure. The code is parallelized and vectorized: Each subdomain is associated to one vectorial processor. Details may be found in [11].

For the spatial development study, a sphere is embedded within the computational domain. The modeling of the sphere makes use of a 'pseudo-penalization technique' [12], *i.e.*, a penalization term is *implicitly* introduced in the momentum equations to approximately cancel the velocity inside the sphere. The temperature is let free to evolve, *i.e.* the sphere material is assumed thermally conductive. For simplification, the fluid and the sphere thermal diffusivities are taken equal, so that the fluid temperature equation also holds inside the sphere, where then one solves the heat equation. One may indeed think that the sphere conductivity has a negligible impact on the far wake.

2.3. The SVV–LES technique

To compute turbulent flows we use a LES approach, based on a stabilization technique, such that the 'spectral accuracy' of the approximation is preserved. It relies on the introduction in the governing equations of a dissipation term only active in the highest Fourier and Chebyshev frequency ranges. In the 1D 2π-periodic case, when using the Fourier approximation, such a term, say V_N, is such that its Fourier spectrum is:

$$(\widehat{V}_N)_k = -\epsilon_N \widehat{Q}_k k^2 (\hat{u}_N)_k \quad -N \leqslant k \leqslant N$$

where u_N is the trigonometric polynomial interpolant of degree N that approximates some exact solution u. In this formula ϵ_N is a $O(N^{-1})$ parameter and the $\widehat{Q}_k$ a set of coefficients such that $\widehat{Q}_k = 0$ if $k \leqslant m_N$ and $1 \geqslant \widehat{Q}_k > 0$ if $k > m_N$, with *e.g.* the threshold value $m_N = O(\sqrt{N})$, see [13] for a theoretical analysis carried out on the inviscid Burgers equation.

In Fig. 1 we show the variations of $\widehat{Q}_k$ with respect to k/N, for two different values of m_N and using $\widehat{Q}_k = \exp(-((k-N)/(k-m_N))^2)$, as suggested in [14] where the non-periodic spectral Legendre case is investigated. The SVV stabilization may be compared to the Chollet–Lesieur (C–L) spectral viscosity, which is a LES closure expressed in spectral space derived from the Eddy-Damped Quasi-Normal Markovian (EDQNM) theory [15]. It is remarkable to observe that the main difference between C–L and SVV lays in the fact that C–L is active on the full spectrum, whereas SVV only acts on the high frequencies. With respect to C–L, SVV may be viewed as a modeling restricted to the high frequency range, in the spirit of Variational Multi Scales (VMS) methods that have been recently developed, see *e.g.* [16]. Note that from Chollet–Lesieur theory one can also derive the following amplitude coefficient of the dissipation term: $\epsilon_N \sim N^{-4/3}$. It is also of interest to compare SVV and hyperviscosity. If we assume that hyperviscosity is implemented through a bi-Laplacian, then in Fourier space we have:

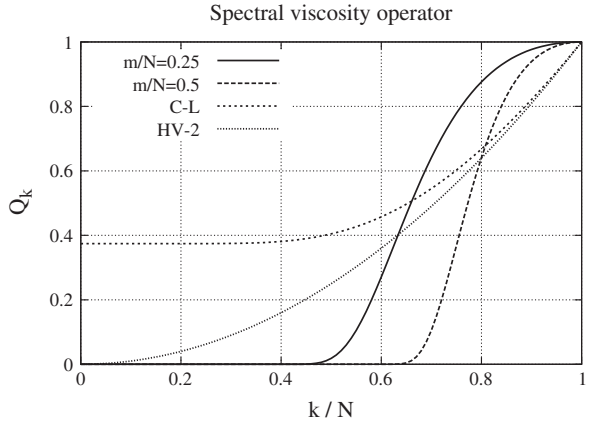

Fig. 1. Spectral viscosity operator for two different thresholds m_N. Comparisons with the Chollet–Lesieur spectral viscosity (C–L) and with an hyperviscosity stabilization (HV-2).

$$-(\widehat{\Delta^2 u_N})_k = -k^4(\hat{u}_N)_k = -\widehat{Q}_k k^2(\hat{u}_N)_k, \quad \widehat{Q}_k = k^2$$

We have also reported this parabola in Fig. 1. We note that for $k/N \approx 1$, C–L and hyperviscosity provide similar hyperviscous behaviors (the two curves show the same slope), whereas SVV acts like a Laplace operator (the slope vanishes).

Extending this approach to the multidimensional vector case is not a trivial task, see *e.g.* [17] for the Navier–Stokes equations and [18] in the frame of LES. Details of our approach have already been described, see *e.g.* [19–21]. Note that we use a similar stabilization for both the velocity components and for the temperature. Concerning the optimal values of the SVV parameters, we refer to [22] where, on the basis of numerical experiments, it appears suitable to simply minimize the SVV contribution together with preserving the stability of the scheme.

3. Spatial development study

The computation is done in the Galilean frame of reference of the sphere and at the initial time the temperature gradient is constant. For the boundary conditions: (i) at the inlet of the channel the velocity and temperature gradient are constant, (ii) at the horizontal boundaries one assumes free-slip conditions for the velocity and adiabaticity for the temperature, (iii) the flow is periodic in transverse direction and (iv) at the outlet one uses an advection equation at the (constant) bulk flow velocity.

The computational domain is $\Omega = (-4.5, 30.5) \times (-4, 4) \times (-4, 4)$ and the sphere, of unit diameter, is centered at the origin, see Fig. 2. In streamwise direction we have eight subdomains of variable length, with interfaces located at $x = \{-4.5, -0.5, 0.5, 2.5, 6.5, 12.5, 18.5, 24.5\}$ in order to accumulate grid points just upstream and downstream of the sphere. In each subdomain, the polynomial approximation degrees equal $N_x = 60$ and $N_y = 160$, and we use $N_z = 80$ Fourier modes. Then we have about 12 millions of grid points for this simulation. The SVV parameters are taken equal to $\epsilon_N = 1/N$, $m_N = N/2$ for the velocity and $m_N = \sqrt{N}$ for the temperature. This smaller value of m_N has been used for stability reasons in the temperature calculation. The space computation was carried out till time $t_F = 190$ (reference time, D/U), with a time-step $\tau = 5 \times 10^{-3}$.

Fig. 3 shows some first and second order statistics, computed during the last 60 time units, both for the velocity and temperature. The streamwise velocity mean profiles show that, in the near wake and for $F = 25$, the influence of the stratification may be neglected, since the y- and z-profiles coincide. This is *e.g.* coherent with the experiments of [3], where a Re–F diagram shows that for $Re = 10^4$ and $F > 20$, the velocity–temperature coupling is negligible at such small distances from the sphere. The anisotropy of the flow is only pointed out by the temperature variance profiles. Moreover, the maxima of the turbulent kinetic energy are decreasing downstream of the sphere whereas at the considered distances the temperature variance profiles are still increasing. Note that such profiles are not completely converged, so that one can observe some symmetry deficiencies. However our goal is not to get fully converged statistics but instantaneous temperature and velocity fields, to be used as relevant initial conditions for the temporal study.

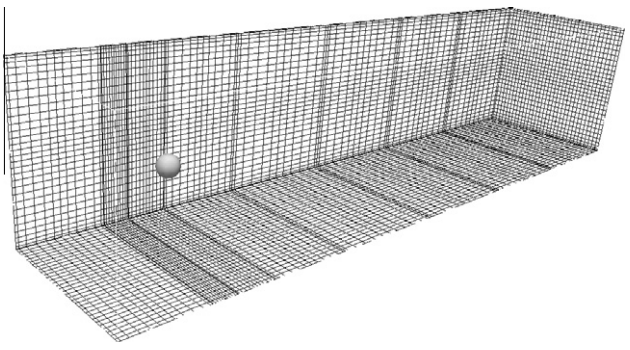

Fig. 2. Schematic of the mesh for the spatial study, visualizing 1 point for 5 in each direction. In both x and y-directions mappings are applied to accumulate grid points close to the sphere.

To conclude this section we provide some details on the sphere modeling, using the pseudo-penalization technique. Thus, Fig. 4 (left) shows the mean steamwise velocity along the streamwise direction. The minimum of u_x is found at $x = 1.46$, with value $u_x = -0.364$. This is *e.g.* coherent with the result obtained in [23], for a non-stratified fluid and using a 5th order accurate LES based on the dynamic Smagorinsky model. A zoom inside the sphere is provided in Fig. 4 (right), which shows the mean profiles of each component of the velocity along the corresponding diameter, *e.g.* u_x along the x-axis. Such visualizations reveal at best the deficiencies of our penalization technique and it has been checked that inside the sphere the fluctuations of the velocity components were negligible, so that it is relevant to look at the time averaged values. Mainly, one remarks some oscillations of the streamwise velocity just behind the blocking point at the sphere front. Globally, the agreement of our results with the theoretical analysis which predicts a $O(\tau)$ residual velocity appears however satisfactory.

4. Temporal development

Since computing the space development in a domain of excessive length, say $2500D$, is out of reach of the present computer capabilities, we plan now to carry out a time development study, starting from the result of the space development study. To this end, we focus on the following x-truncated subdomain of Ω: $(6.5, 24.5) \times (-4, 4) \times (-4, 4)$, which corresponds to the 5th, 6th and 7th subdomains, see Fig. 2, and plan to see, now in a fixed frame of reference, how this part of the wake evolves in time. First, because temporal studies usually assume periodicity in streamwise direction, the observed part of the wake must be made periodic in x-direction. Second, because we expect a large increase of the wake width in the median horizontal plane, due to the confinement effect of the stratification, the computational domain must be enlarged. Finally, we propose using a divergence cleaning like method to get a divergence free initial condition and thus a well posed Navier–Stokes problem. The approach that we suggest shows the following steps:

- The streamwise velocity is corrected by the sphere velocity, plus a small adjustment to take into account that the spatial computation was not carried out in an open domain (in dimensionless form we used $U = 1.0038$). The adjustment is required to take into account the flow drained by the sphere: Due to the incompressibility constraint, using a unitary correction would induce a non zero velocity at the artificial boundary of the computational domain Ω. With such an adjustment, we cancel at best the velocity at the artificial boundaries. Out of the wake the flow is then at rest.
- In streamwise direction the flow is embedded in a twice larger domain and made periodic by symmetrically extending the velocity components and temperature fields. More precisely, we use even symmetries of u_x, u_y, u_z and T, such that $6.5 < x < 24.5$, with respect to the plane $x_0 = 24.5$. Since the streamwise direction becomes the homogeneous one, for the temporal study the x-direction is handled with Fourier expansions and the z-direction with the Chebyshev multi-domain method. Then one has to transfer the data obtained on the space

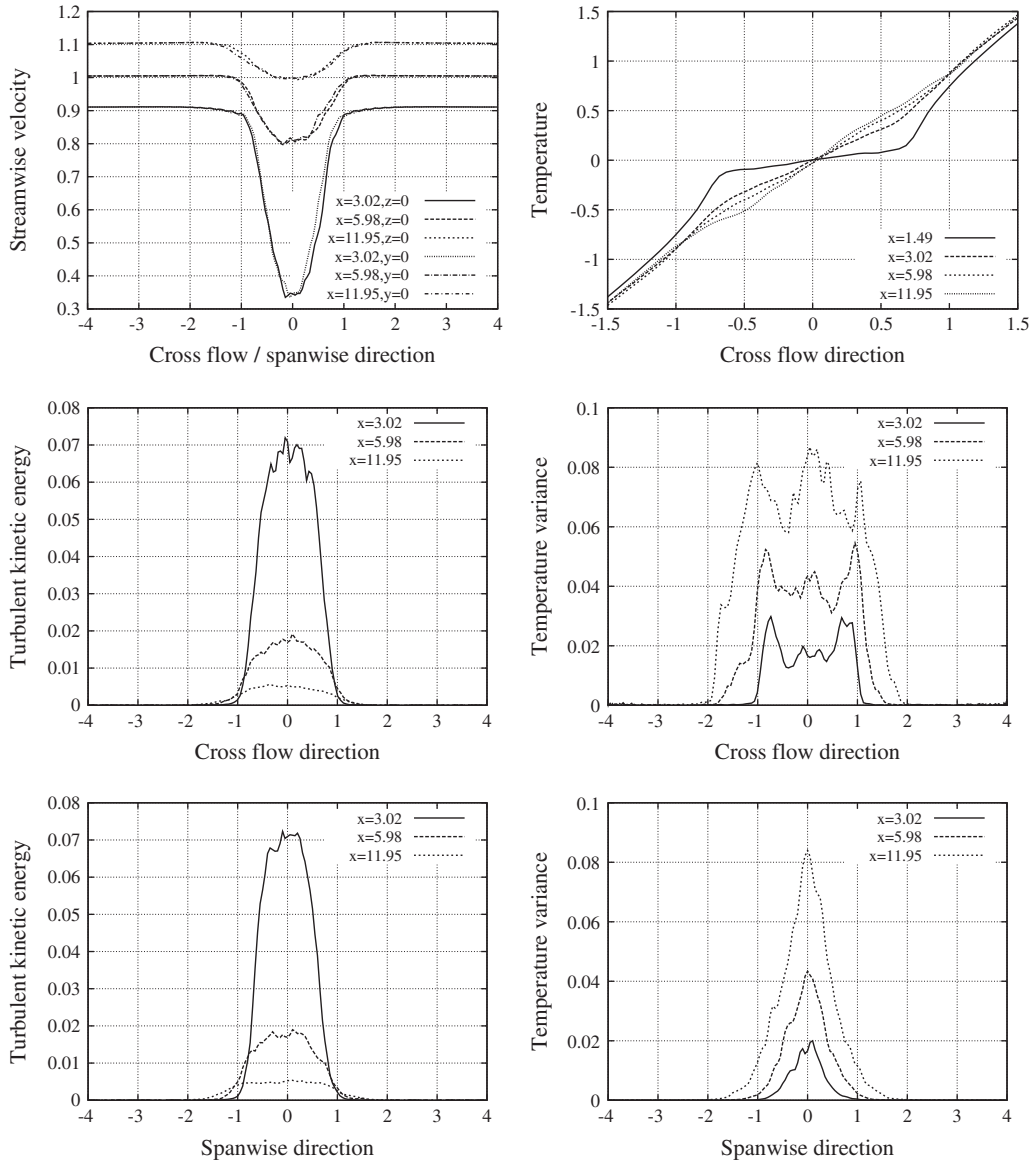

Fig. 3. Mean profiles of streamwise velocity (with a ±0.1 shift) and temperature at different abscissa. Turbulent kinetic energy and temperature variance along the vertical (y) and transverse (z) directions.

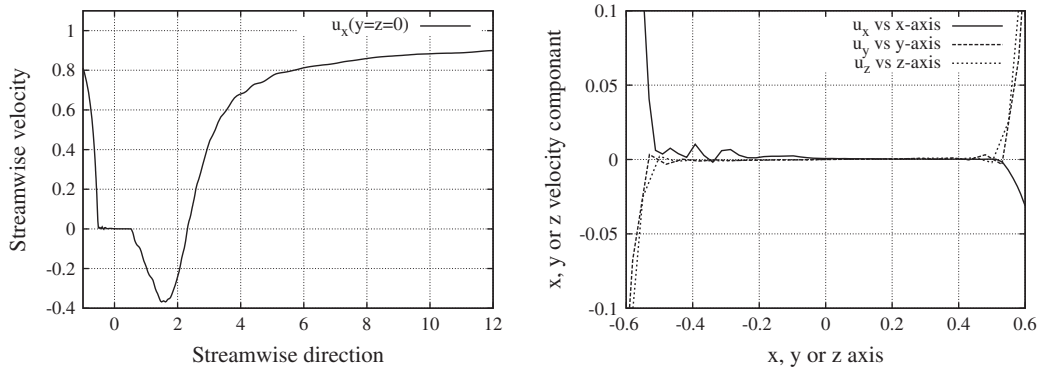

Fig. 4. Mean streamwise velocity versus the longitudinal axis ($y = 0$, $z = 0$) (at left) and velocity components u_x, u_y and u_z versus the x, y and z-axis, respectively (at right).

computational grid to the temporal one. This is done by using a Chebyshev interpolation, to go from the non-regular Gauss–Lobatto–Chebyshev (plus mapping) mesh to the regular Fourier one, and by using a trigonometric interpolation for the inverse.

– In the horizontal transverse direction the flow is embedded in a three times larger computational domain, in which the temperature and velocity fields are extended by the profiles obtained at the end of the space development computation.

– The extended velocity field is made divergence free by projection onto a space of divergence-free vectors, as it is classical with fractional step methods. Note indeed that after the symmetrization and with $\tilde{\boldsymbol{u}}$ for the extended velocity field, $\nabla\cdot\tilde{\boldsymbol{u}} = 2\partial_x\tilde{u}_x$ in the streamwise extended part. This results from the fact that the symmetry preserves the derivatives in y and z, but gives the opposite for the derivative in x. The "divergence cleaning" procedure consists in computing $\boldsymbol{u} = \tilde{\boldsymbol{u}} + \nabla\varphi$, where φ solves the Poisson equation $\Delta\varphi = -\nabla\cdot\tilde{\boldsymbol{u}}$ with an homogeneous Neumann boundary condition. However, taking advantage of the fact that our Navier–Stokes solver makes use of a projection method and since we know the velocity and temperature fields at the previous time levels, we actually use a slightly improved algorithm: The computation is restarted with the three time level BDF2 scheme, using the temperature and velocity fields obtained by symmetry, and the projection is carried out by the solver at the end of the first time-step. Since the Navier–Stokes equations are not verified in the part constructed by symmetry, again due to the change of sign in the first order x-derivatives, we then implicitly introduce during the first time-step a compensatory forcing. This forcing term may be viewed as the force field required at the beginning of the simulation to enforce the periodicity.

After translation in x, we thus obtain the domain $\Omega' = (-18, 18)\times(-4,4)\times(-12,12)$, within which the velocity and temperature fields are completely defined. Fig. 5 shows the result of this periodic extension algorithm for the temperature field, which are visualized at the end of the space development computation and at the beginning of the temporal one. Note that thanks to an additional translation the space development result has been centered inside Ω'. This has of course no influence on the ulterior development of the flow.

Fig. 6 shows the components of the velocity field at the beginning of the time development study. Thanks to using even symmetries (i) the velocity remains continuous (C^0 continuity) and (ii) the direction of the flow drained by the sphere is preserved, *i.e.* along the x-axis u_x keeps the same sign in the initial and extended part. Any other kind of set up of the initial condition would yield an unphysical flow, showing *e.g.* discontinuities of the velocity components. Thus, the flow that would be obtained by reflection (Navier–Stokes equations are preserved by reflection), *i.e.* with respect to the plane $x = x_0$ such that $\tilde{u}_x(x,.) = -u_x(2x_0 - x,.)$, $\tilde{u}_y(x,.) = u_y(2x_0 - x,.)$, $\tilde{u}_z(x,.) = u_z(2x_0 - x,.)$, would be unphysical. Note however that the present procedure does not avoid discontinuities of the first order derivatives (C^1 discontinuity), then inducing some high frequencies. One may think that the SVV technique helps to damp these frequencies.

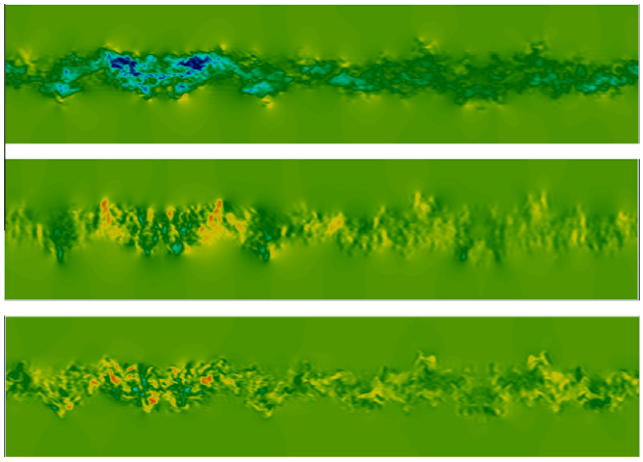

Fig. 6. Instantaneous velocity components at the beginning of the time development computation ($t = 191$). The color map is the same as in Fig. 5 with extrema ±0.5 for the three components. From up to down: Streamwise (u_x), vertical (u_y) and transverse (u_z) velocity components.

One may fear that a long time interval is required to smooth the perturbation associated to the transition from the space to the temporal study. Fig. 7 shows the variations in time of the residual of the vertical component of velocity, u_y, and of the temperature, T, around the transition time $t = 190$. The residuals are defined similarly for u_y and T, *e.g.* for the temperature $r_T = \max|\delta T|/\tau$, where δT is the difference between two consecutive temperature fields (τ is the time-step). First, one observes that the levels of the space and time studies residuals are very different. For the temporal study the flow indeed simply relaxes whereas for the spatial one, carried out in the Galilean frame of the sphere, it is strongly unsteady, especially due to the vortex shedding. Second, one observes a peak at the first time-step of the temporal study. This is associated to the projection procedure and to the change of computational grid. However, it appears that beyond this first time-step no spurious perturbation survives.

5. Results

The temporal computation has been carried out in $\Omega' = (-18, 18)\times(-4,4)\times(-12,12)$, using free-slip condition and adiabaticity at all side walls, except those orthogonal to the homogeneous

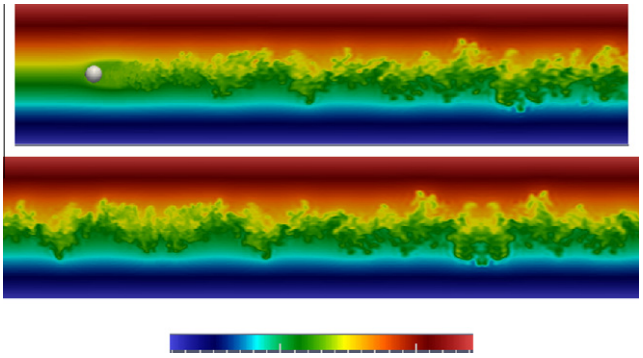

Fig. 5. Instantaneous temperature fields, at the end of the space development study ($t = 190$) and at the beginning of the time development computation ($t = 191$), using the above color map with $-4 \leqslant T = y \leqslant 4$. In streamwise x-direction the temperature field is discretized on a multi-domain Chebyshev mesh in the first figure, whereas in the second one it is defined on a regular Fourier grid.

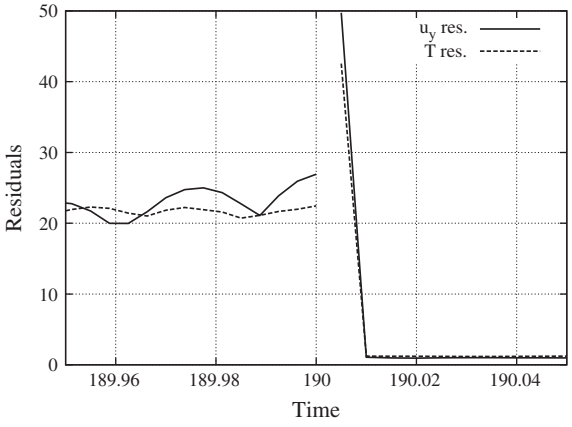

Fig. 7. Variations in time of the residuals of the vertical velocity and temperature at the end of the spatial study and at the beginning of the temporal one ($\tau = 5\times10^{-3}$).

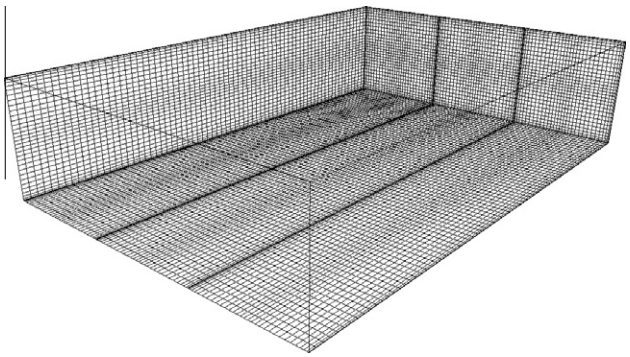

Fig. 8. Schematic of the mesh for the temporal study, visualizing 1 point for 5 in each direction. One uses now the regular Fourier grid in x-direction and the multi-domain Chebyshev one in transverse z-direction.

x-direction. For the discretization we use three identical subdomains (now in z-direction), with $N_x = 180$ Fourier modes, $N_y = 160$ and $N_z = 159$ in each of them. This yields about 27,705,000 grid points, see Fig 8.

SVV parameters have been taken equal to $m_N = N/2$ and $\epsilon_N = 1/N$. The flow has been computed from $t = 190$ till $t = 2652$, the time-step being increased from $\tau = 5 \times 10^{-3}$ till $\tau = 0.16$. However, it is relevant to relate the initial time of the temporal study to the distance to the sphere, *i.e.* to $t = (6.5 + 24.5)/2 = 15.5$, resulting in a time shift of 174.5. Moreover, the relevant time scale is now the inverse of the buoyancy frequency, so that the dimensionless time must be scaled with the Froude number $F = 25$. Thus, the temporal study was carried for $0.62 < Nt < 99.1$ (here t has a dimension and Nt is the dimensionless time). Note that it would not be satisfactory to go on the computation beyond this final time, due to confinement effects both in streamwise and transverse directions.

Fig. 9 shows visualizations at different times of the temperature and transverse vorticity ω_z in the vertical median plane $z = 0$, together with the vertical vorticity ω_y in the median horizontal plane $y = 0$. One clearly discern the increasing width of the wake in the horizontal plane and the confinement effect, with appearance of the so-called pancake eddies, in the vertical one. Note that such figures may recall those of [10] ($Re = 10^4$, $F = 10$), but at much shorter times; Thus, our visualization at $Nt = 99.1$ reminds their result at $Nt = 675$. One may then think that the presence of coherent vortex structures at the initial time induces a quicker development of the

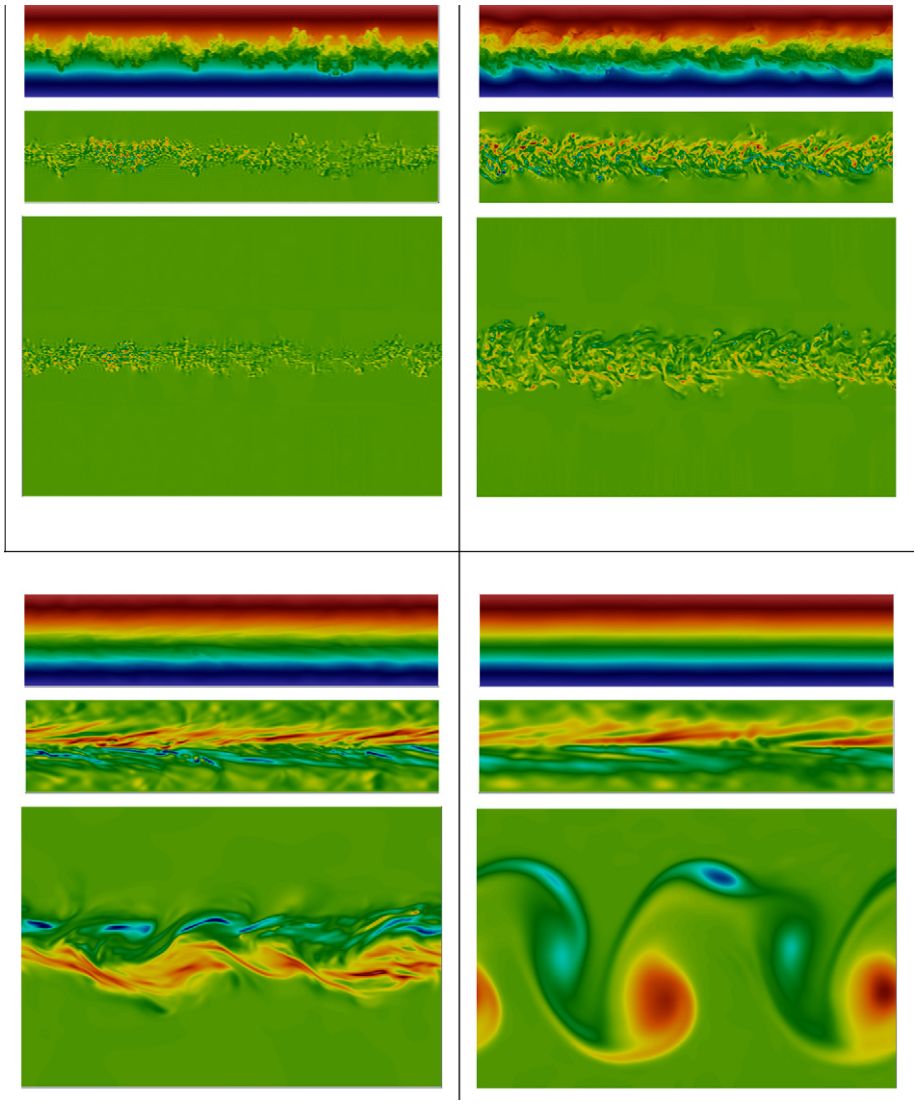

Fig. 9. Instantaneous temperature and vorticity fields at times $Nt = \{0.66, 5.66, 24.86, 99.1\}$ (from left to right and up to down). In each quadrant, from up to down: Temperature in the median vertical plane, with $|T| \leqslant 4$; Transverse component of the vorticity in the same plane, using the time-dependent scaling $|\omega_z| \leqslant \{5.3, 0.46, 0.089, 0.026\}$; Vertical component in the horizontal plane, using $|\omega_y| \leqslant \{6.9, 0.65, 0.063, 0.021\}$. For all figures the color map is the one used in Fig. 5.

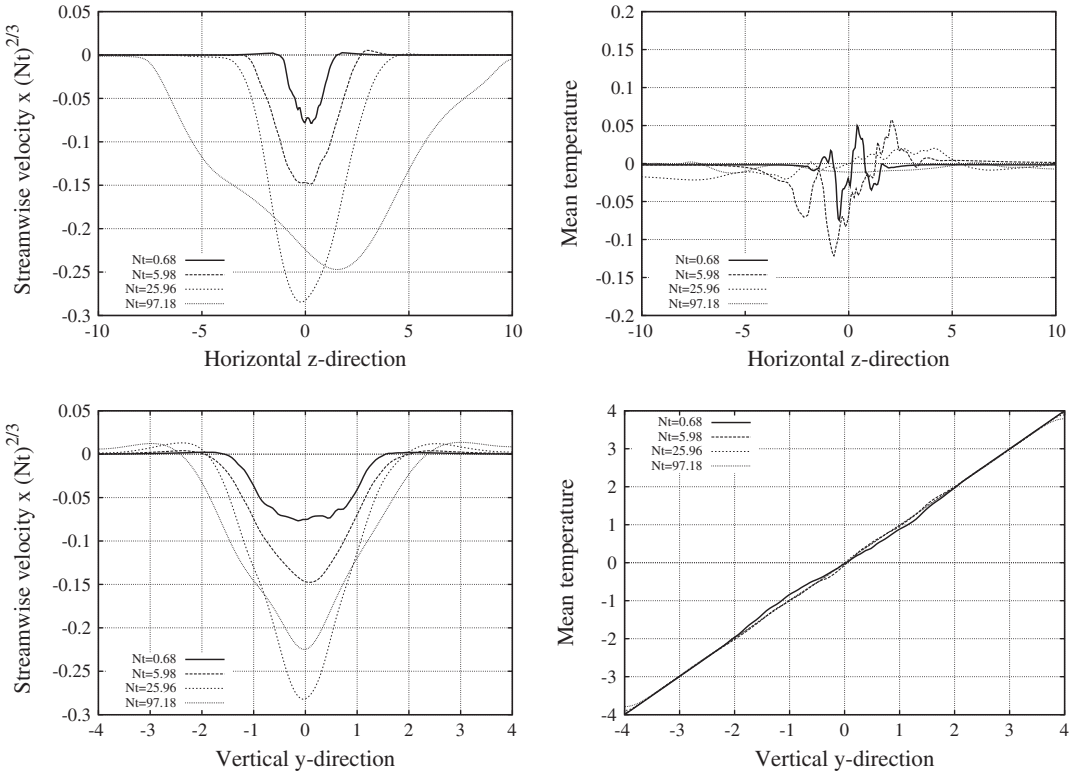

Fig. 10. Mean streamwise velocity times $(Nt)^{2/3}$ and temperature in median transverse (z) and median vertical (y) directions at different times (note that the scales in z and y differ by a factor 10/4).

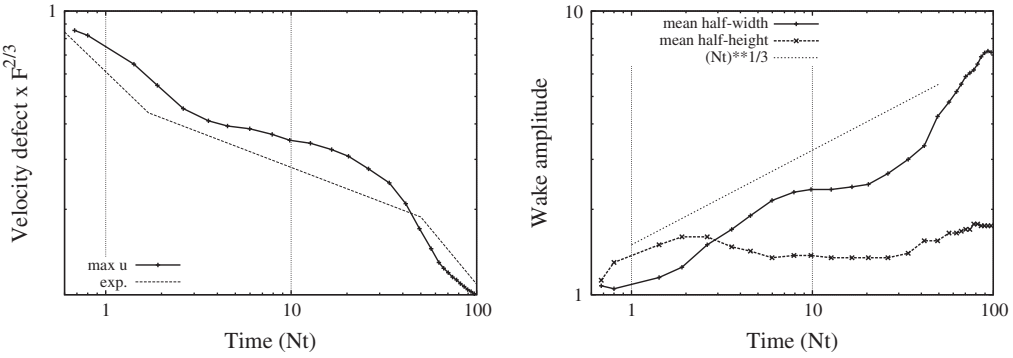

Fig. 11. Evolution of the $F^{2/3}$ weighted velocity defect (at left) and wake amplitude (width and height) (at right). Comparisons with the 'universal curve' and predictions of [24].

Table 1
Decrease rates and critical Nt values for the LES and the experiments. Nt_I (resp. Nt_{II}) separates the 3D and NEQ (resp. NEQ and Q2D) regimes.

	Nt_I	Nt_{II}	Rate 3D	Rate NEQ	Rate Q2D
[24]	1.7 ± 0.3	50 ± 15	−2/3	−0.25 ± 0.04	−0.76 ± 0.12
SVV–LES	2.4	30	∼−2/3	−0.2	∼−0.76

stratified wake even if, as claimed in [8–10], the seeding of coherent vortex structures is not required to observe the formation and development of far-wake eddies. Note however that the definition of a reference length is not obvious when no obstacle is present, so that the Reynolds and internal Froude number values may then be discussed.

More quantitative results are given in Fig. 10, where mean profiles of the temperature and streamwise velocity are displayed. The velocity profiles are weighted by $(Nt)^{2/3}$, knowing that in the non-stratified case the velocity defect decreases as $(Nt)^{-2/3}$. These mean profiles result from a space averaging, in streamwise direction, together with a (non-weighted) time averaging during 600 time-steps during the temporal development. The time value affected to each curve corresponds to the median one during this laps of time. The statistics are of course not well converged, but they clearly show the confinement effect in vertical direction and the wake width increase in transverse direction.

The temperature profiles show a slow return to a quasi-linear stratification. From the velocity profiles one can provide the temporal evolution of the velocity defect and of the amplitude of the wake, see Fig. 11. The velocity defect is computed from the minimum of the mean streamwise velocity in the median horizontal plane. For the amplitude of the wake, we also use space and time averaged values and, as suggested in [24], the wake region is defined as the band where the velocity defect exceeds 20% of its

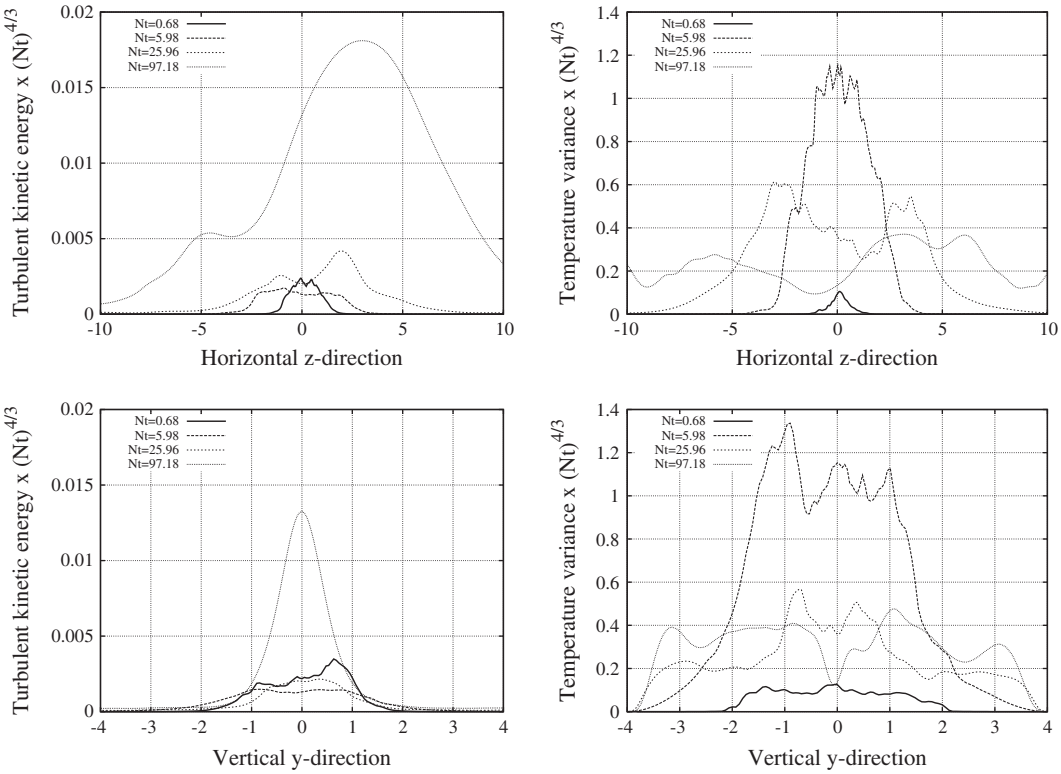

Fig. 12. Turbulent kinetic energy and temperature variance times $(Nt)^{4/3}$ in median transverse (z) and median vertical (y) directions at different times.

maximum. Note that Gaussian fits are often used to define such amplitudes, but when starting from a non *ad hoc* initial condition, such profiles are only poorly Gaussian, see Fig. 10. As expected from the works of [24], the variation in time of the velocity defect clearly shows three regimes. Thus, we find the '3D' (three-dimensional), the 'NEQ' (non-equilibrium) and the 'Q2D' (quasi-two-dimensional) regimes, for low, intermediate and high values of Nt, respectively. It is worth noting that the experimental curve summarizes a large amount of experimental results, obtained for various values of the Froude and Reynolds numbers. The dependence on the Froude number is taken into account by the $F^{2/3}$ weight whereas the dependence on the Reynolds number is negligible, for sufficiently high values of these two control parameters. Finally, it may be checked, *e.g.* by looking at the Fig. 7 of [8], that the transitional NEQ regime seems to appear clearer in the present simulations than in previous numerical works.

Comparisons between the present LES results and the experimental 'universal curve' of [24], for both the ranges and the slopes, are provided in Table 1. The ranges only slightly differ from the experiments. Concerning the rates of decrease, in the 3D and Q2D regimes it is difficult to get a precise approximation of the slopes, see Fig. 11 (left), but one may consider that our results are satisfactory. In the NEQ regime, the LES rate is slightly lower (in absolute value) than the experimental one.

Concerning the time variations of the wake width, from [24] one should recover the rate of the non-stratified case, *i.e.* 1/3. In the mean we indeed obtain such a rate, see Fig. 11, but large fluctuations are present: For $Nt \approx 10$ the rate is close to 0 whereas for $Nt \approx 50$ it is close to 1. Concerning the wake height the variations are much smaller: One first observes a maximum, for $Nt \approx 2$, *i.e.* at the transition of the 3D and NEQ regimes. Beyond that, the stratification becomes active: The wake height slightly decreases and then remains constant during the NEQ range, before increasing slowly again during the Q2D regime. Such results conform with the experiments reported in [25], where some wide minima also appear in the NEQ range, depending on the internal Froude number value.

We finish the paper with some second order statistics, using again an average in streamwise direction together with an average over 600 time-steps. Fig. 12 shows the turbulent kinetic energy and the temperature variance, both weighted by $(Nt)^{4/3}$. This weight is again based on the non-stratified case, for which the velocity fluctuations as well as the fluctuations of a passive scalar decrease as $(Nt)^{-2/3}$. The distortion with respect to the non-stratified case is especially pointed out by the great amplitude of the turbulent kinetic energy profile at $Nt = 97.18$.

6. Conclusion

The problem of the computation of the stratified far wake of a sphere has been revisited, using a highly accurate SVV stabilized spectral LES and a temporal/spatial procedure. The approach is based on first carrying out a spatial development study to establish a relevant initial condition to the temporal one, so that it does not suffer from setting up an artificial initial condition as done in previous numerical works. The critical point is to carefully transfer the results from the spatial to the temporal study. A periodic extension algorithm has been suggested to this end, which may be used in different contexts, *i.e.* for different physical problems and using different numerical methods. Since the only fully satisfactory procedure would be to carry out a spatial development study in a computational domain of excessive size, such an approach remains not perfect but is from our point of view much better than the more academical temporal study. The present temporal/spatial SVV–LES has allowed the computation of the turbulent wake of a sphere, in thermally stratified water, at distances of about 2500 diameters. Experimental results have been recovered in rather satisfactory way, especially showing the three expected flow regimes

(3D, NEQ and Q2D) and the confinement effect due to the stratification.

Acknowledgments

Computations were done on the computer NEC-SX8 of the IDRIS computational center (Projects 074055 and 094055). We thank the CTSN (Toulon Navale) for his support.

References

[1] Lin JT, Pao YH. Wakes in stratified fluids. Annu Rev Fluid Mech 1979;11:317–38.
[2] Riley JJ, Lelong MP. Fluid motions in the presence of strong stable stratification. Annu Rev Fluid Mech 2000;32:613–57.
[3] Lin QL, Lindberg WR, Boyer DL, Fernando HJS. Stratified flow past a sphere. J Fluid Mech 1992;240:315–54.
[4] Chomaz JM, Bonneton P, Hopfinger EJ. Structure of the near wake of a sphere moving in a stratified fluid. J Fluid Mech 1993;253:1–21.
[5] Chashechkin YD. Hydrodynamics of a sphere in a stratified fluid. Fluid Dyn 1989;24(1):1–7.
[6] Spedding GR, Browand FK, Fincham AM. Vertical structure in stratified wakes with high initial Froude number. J Fluid Mech 1996;23:171–82.
[7] Bonnier M, Eiff O, Bonneton P. On the density structure of far-wake vortices in a stratified fluids. Dyn Atmos Oceans 2000;31:117–37.
[8] Diamessis PJ, Domaradzki JA, Hesthaven JS. A spectral multidomain penalty method model for the simulation of high Reynolds number localized incompressible stratified turbulence. J Comput Phys 2005;202:298–322.
[9] Dommermuth DG, Rottman JW, Innis GE, Novikov EV. Numerical simulation of the wake of a towed sphere in a weakly stratified fluid. J Fluid Mech 2002;473:83–101.
[10] Gourlay MJ, Arendt SC, Fritts DC, Werne J. Numerical modeling of initially turbulent wakes with net momentum. Phys Fluids 2001;13(12):3783–802.
[11] Cousin L, Pasquetti R. High-order methods for the simulation of transitional to turbulent wakes. In: Lu Y, Sun W, Tang T, editors. Advances in scientific computing and applications. Beijing/New York: Sciences Press; 2004. p. 133–43.
[12] Pasquetti R, Bwemba R, Cousin L. A pseudo-penalization method for high Reynolds number unsteady flows. Appl Numer Math 2008;58:946–54.
[13] Tadmor E. Convergence of spectral methods for nonlinear conservation laws. SIAM J Numer Anal 1989;26(1):30–44.
[14] Maday Y, Kaber SMO, Tadmor E. Legendre pseudo-spectral viscosity method for nonlinear conservation laws. SIAM J Numer Anal 1993;30(2):321–42.
[15] Chollet JP, Lesieur M. Parameterisation of small scales of three-dimensional isotropic turbulence utilizing spectral closures. J Atmos Sci 1981;38:2747–57.
[16] Hugues TJR, Mazzei L, Oberai AA. The multiscale formulation of large eddy simulation: decay of homogeneous isotropic turbulence. Phys Fluids 2001;13(2):505–12.
[17] Kirby RM, Sherwin SJ. Stabilisation of spectral/hp element methods through spectral vanishing viscosity: application to fluid mechanics modelling. Comput Methods Appl Mech Eng 2006;195:3128–44.
[18] Karamanos GS, Karniadakis GE. A spectral vanishing viscosity method for large-eddy simulation. J Comput Phys 2000;163:22–50.
[19] Xu CJ, Pasquetti R. Stabilized spectral element computations of high Reynolds number incompressible flows. J Comput Phys 2004;196(2):680–704.
[20] Pasquetti R. Spectral vanishing viscosity method for large-eddy simulation of turbulent flows. J Sci Comput 2006;27:365–75.
[21] Minguez M, Pasquetti R, Serre E. High-order large-eddy simulation of flow over a simplified car model. Phys Fluids 2008;20:095101.
[22] Pasquetti R. Spectral vanishing viscosity method for LES: sensitivity to the SVV control parameters. J Turbul 2006;6(No 12):1–14.
[23] Contantinescu G, Squires K. LES and DES investigations of turbulent flow over a sphere at re = 10,000. Flow Turbul Combust 2003;70:267–98.
[24] Spedding GR, Browand FK, Fincham AM. The evolution of initially turbulent bluff-body wakes at high internal Froude number. J Fluid Mech 1997;337:283–301.
[25] Spedding GR. Vertical structure in stratified wakes with high initial Froude number. J Fluid Mech 2002;454:71–112.